

## Determination of performance characteristics using FEA-analytical for outer rotor BLDC motor

Saharudin Kamaroszaman<sup>1,2</sup>, Raja Nor Firdaus Kashfi Raja Othman<sup>1,2</sup>, Kasrul Abdul Karim<sup>1,2</sup>,  
Suhairi Rizuan Che Ahmad<sup>3</sup>, Kunihi Tashiro<sup>4</sup>

<sup>1</sup>Fakulti Kejuruteraan Elektrik, Universiti Teknikal Malaysia Melaka, Durian Tunggal, Melaka, Malaysia

<sup>2</sup>Electrical Machine Design Research Laboratory, Centre of Robotics & Industrial Automation, CeRIA, UTeM, Melaka, Malaysia

<sup>3</sup>Electrical Technology Section, Universiti Kuala Lumpur Kampus Cawangan British Malaysian Institute, Kuala Lumpur, Malaysia

<sup>4</sup>Faculty of Engineering, Shinshu University, Nagano, Japan

### Article Info

#### Article history:

Received May 10, 2023

Revised Jul 10, 2023

Accepted Jul 28, 2023

#### Keywords:

BLDC

FEA

Motor design

Outer rotor

Performance curve

### ABSTRACT

This paper presents an analytical approach to determine the performance characteristics of an outer rotor brushless DC (BLDC) motor using finite element analysis (FEA). An accurate performance characteristic is a crucial deliverable during the early motor design process in order to minimize the cost of change while delivering a feasible design to the application. There are several popular methods to determine motor performance, including template-based software as well as FEA. However, these two methods have limitations in terms of geometry and time. Therefore, this paper proposes that the limitations can be addressed by using a combination of FEA and mathematical equations. First, the optimum motor design is determined using an FEA analytical approach. Second, the torque constant  $K_T$ , is derived from the FEA results and followed by performance curve generation using the mathematical equation of speed, current, and output power in terms of torque function. Finally, the outcome results are verified against the motor requirements, including an assessment of maximum speed, stall current, and maximum output power. In conclusion, this research introduces a methodology for determining full curve motor performance prior to prototype fabrication. The leverage benefit could be gained through robust design and low-cost development.

This is an open access article under the [CC BY-SA](#) license.



### Corresponding Author:

Raja Nor Firdaus Kashfi Raja Othman

Fakulti Kejuruteraan Elektrik, Universiti Teknikal Malaysia Melaka

76100 Durian Tunggal, Melaka

Email: norfirdaus@utem.edu.my

## 1. INTRODUCTION

Brushless DC (BLDC) motors are widely used in industrial applications worldwide due to their benefits in terms of high torque, light weight, noiseless operation, and high efficiency [1], [2]. Furthermore, the precision of the BLDC motor allows industrial players to reduce their energy consumption and heat generation, resulting in a longer operating life [3]–[6]. In high torque applications, the outer rotor BLDC (ORBLDC) motor is one of the best motor candidates due to its high torque density characteristic profile and low manufacturing cost [7]–[11].

To sustain BLDC motor market demand, engineers must design motors with optimal performance but within a short time frame and at an acceptable development cost. Therefore, upfront simulation is very important in motor design process, and the full curve motor performance estimation is one of it [12]. The estimation curve is required by the motor designer to run the feasibility design process and compare it against

the application requirement [13], [14]. Since most applications require dynamic motor performance in torque and speed, it is essential to ensure all the operating points fall within the appropriate zone of the curve (continuous or intermittent zones). The electromagnetic characteristics of the motor can be changed by changing the wire size or the number of wires turns in the winding, or both. More torque and lower speed motor performance can be achieved with more turns of smaller wire, while less torque and higher speed motor performance can be achieved with fewer turns of larger wire. This custom configuration can optimize motor performance within product requirements and provide an opportunity for an optimum design solution. Figure 1 shows an example of full curve motor performance, and Table 1 shows the description value.

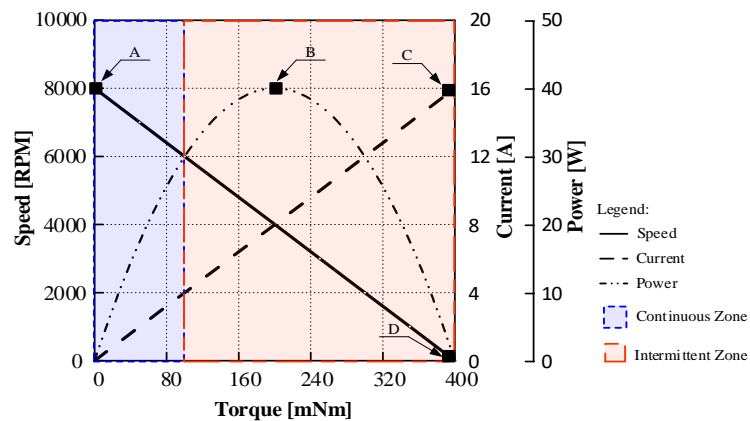


Figure 1. Example full curve performance of BLDC motor

Table 1. Example parameter values from the curve

Indicator	Parameter	Units	Description
A	Free running speed	[rpm]	Speed at rated voltage without load
B	Max. output power	[W]	Highest producible electromagnetic power
C	Stall current	[A]	Highest possible current load
D	Stall torque	[Nm]	Highest producible electromagnetic torque

There are several approaches to determine full curve motor performance. The most popular approach is using a template-based electrical machine design tool. The licensed software can be purchased from well-known software providers such as RMXprt from Ansys, MotorWizard from Solidworks and Simcenter SPEED from Siemens. All the template-based software uses analytical approaches and are capable of generating results in a short period of time. The outcome result can be used as a pre-assessment report for the application requirement and to establish an early level of confidence in electrical motor sizing and configuration [15]–[17]. The generated model from template-based software can be assessed using a finite element analysis (FEA) solver in 2D or 3D dimension for further analysis, but there are limitations when it comes to complex or unique design geometry conditions [18], [19].

Another popular approach is to use MATLAB/Simulink software to mathematically model the BLDC motor [20]–[22]. The motor detailed parameter values on stator, rotor, winding, and mechanical must be configured correctly inside the BLDC block prior to coupling the block with the relevant ideal waveform commutation. The block diagram can be extended to be modelled with a more complex motor control system such as speed control or torque control. However, the issue arises when assumptions must be made when defining parameter values within the BLDC block parameter. In this case, this method can be used when the parameters of the BLDC motor are known, and multiple simulations are performed using different control system parameters.

Last but not least is using FEA analysis to produce full curve motor performance [23], [24]. There are two approaches in this process; the first one uses a speed sweep method, and the second one uses a transient run method. Both methods use mechanical motion as a control variable, and the range setting is from a no-load condition to a stall condition. The speed sweep method is simple in a way by just connecting the individual speed points in a steady state condition, whereas the transient run method uses a huge amount of simulation resources but gives the advantage of plotting torque, power, and efficiency within a time function. Although FEA can produce accurate results, it is inefficient in terms of time consumption.

From the preceding discussion, full curve motor performance should be precise at early development because all operating points should fall within the appropriate zoning area. Overestimation prediction will

result in increased costs, while underestimation prediction will result in product failure. Thus, an acceptable confidence level toward the prediction curve is required within the agreed project lead time. Currently, there are three popular methods, namely template-based software, mathematical BLDC model using MATLAB/Simulink, and FEA. Template-based software and mathematical BLDC models are relatively quick methods, but these methods are rigid to specific template design geometry models and are unable to deliver correct predictions for complex or custom design geometry. While the FEA method is relatively accurate for all design geometries. However, it takes a long time to complete all simulation configurations. As a result, filling this gap would require a new prediction method that can provide significant prediction accuracy in any type of design geometries while ensuring deliverable task within an acceptable lead time. To bridge this gap, this paper will present a method to predict the full curve outer rotor BLDC motor performance using a combination of FEA and mathematical equations. The optimum design is gained from the FEA analytical study of the desired motor geometry, and the performance curve is generated from the mathematical equation. The critical torque constant  $K_T$  in the equation will be derived from FEA results, and the outcome results will be verified against the motor requirements.

## 2. RESEARCH METHOD

### 2.1. Overall flow chart

Figure 2 illustrates the overall methodology flow chart that begins with the generation of design specification and ends with motor performance curve. Section 2.2 elaborates how the design specification was developed. Sections 2.3 and 2.4 explain the methodology for CAD and FEM modelling. The FEA approach was used for all electromagnetic analyses on the stator and rotor, and the best design was chosen based on the target values of  $I_{trans} < 6$  A and  $B_{stat} < 1.8$  T. The method allows the motor designer to analyze custom motor designs up to the optimum condition, where the common multiple objectives such as high output power, high efficiency and small volume size could be achieved prior generate the full curve motor performance [25], [26]. Furthermore, the electromagnetic analysis produces a torque constant  $K_T$  value, which serves as the primary constant for calculating full curve motor performance as described in section 2.6.

### 2.2. Design specification flowchart

Figure 3 shows the design specification flowchart, which begins with the selection of the target application and followed by data collection. The required torque and speed were then determined before the flux density and current limit values were confirmed. For good design practice, the flux density value must be kept below the saturation flux value of 1.8 T and the current value has to be kept below the allowable air convection cooling limit of 6 A [27]. Based on this information, a design review was required to determine whether the specification value could be proceeded with or required modification on material limit selection. After establishing a feasible design specification as per Table 2, the values will be used as the top-level requirement figure that must be met throughout the design process.

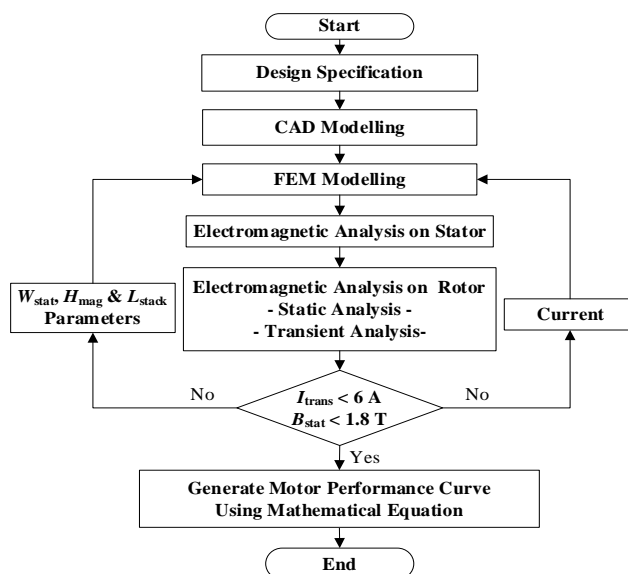


Figure 2. Overall research flowchart

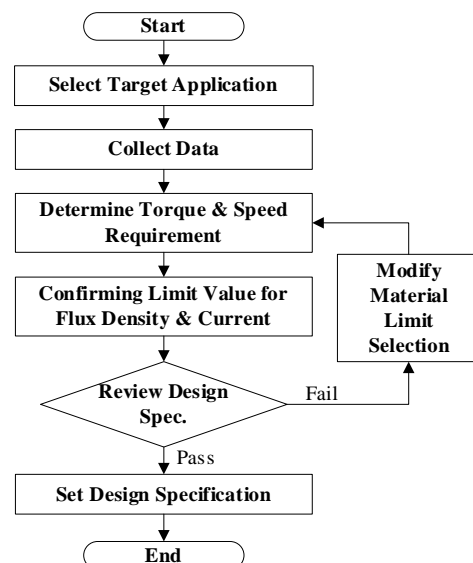


Figure 3. Design specification flowchart

Table 2. Design specification

Parameter	Units	Value
Speed, $n$	[rpm]	< 100
Current, $I$	[A]	< 6
Torque, $T$	[Nm]	35
Flux Density, $B$	[T]	< 1.8

### 2.3. CAD modelling flowchart

As shown in Figure 4, the selection of motor design intent is the initial step in the CAD modeling process, followed by component design. At this stage, the overall number of components could be determined, and the material utilized needs to be identified for an early cost estimation. The assembly process must be considered from the subassembly level all the way up to the final assembly level. During the CAD review, the interference and clearance surface condition will be validated, and any necessary adjustments will be made at component design or sub-assembly design. Upon check all the interaction surface conditions, the CAD model is ready with designated parameter as per Table 3 and variable component name as per Figure 5. At this stage the CAD model is good to be used in FEM modelling. The selection of the stator slot and pole number is fixed based on the finding that the 18 s/20 p configuration delivers the highest output torque with the lowest torque ripple when compared to the 12 s/10 p and 9 s/8 p configurations [28].

### 2.4. FEM modelling flowchart

Figure 6 shows the FEM modelling flowchart that begins with structure modelling process, where the rotating and non-rotating component are declared accordingly. Then the meshing process can be performed by zoning area and element calculation can be proceeded after that. The magnetic analysis only can run after declare material inside FEM software with appropriate configuration. Parameter change must be performed if change in permeance model is not sufficient.

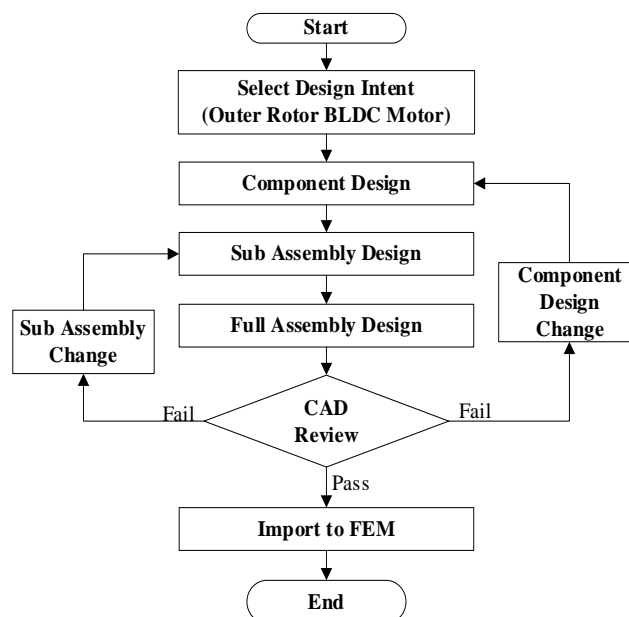


Figure 4. CAD modelling flowchart

Table 3. Motor parameter

Parameter	Units	Value
Slot Number		18
Pole Number		20
Magnet Type		NdFeB
Air Gap	[mm]	1
Winding Diameter	[mm]	1
Winding Fill Slot	[%]	37

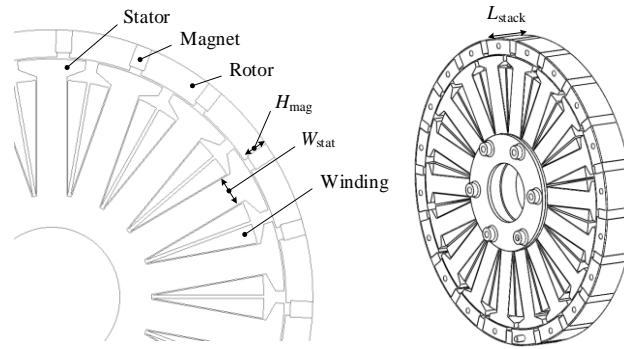


Figure 5. Motor structure

## 2.5. Determine winding turn and winding resistance

Prior proceeding with the full curve performance calculation, there are two constants required, one is torquing constant  $K_T$  that can be determined from electromagnetic analysis and another one is total winding resistance  $R$ , which can be deduced from winding turn estimation. To estimate the turn, an approximate available area for winding is required and this area can be calculated from cross sectional of Single Slot Area  $A_{Slot}$ , as per defined in Figure 7.

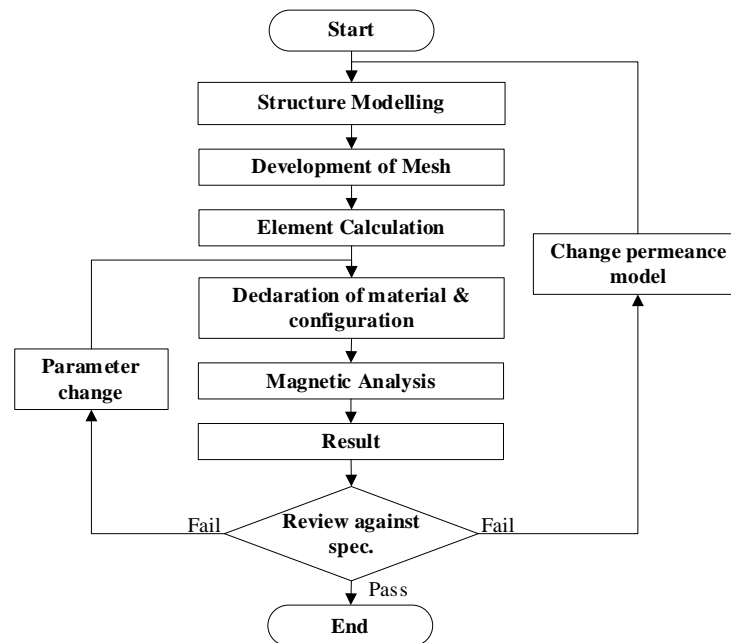


Figure 6. FEM modelling flowchart

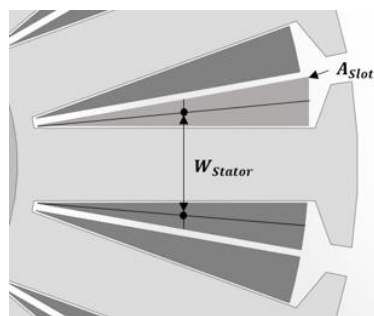


Figure 7. Estimation winding area

The (1) describes how the number of windings turns per slot,  $N$  had been derived from single slot area  $A_{\text{Slot}}$ , Copper Wire Cross Sectional Area  $A_{\text{Wind}}$  and Slot Fill Factor  $K$ . The (2)-(4) show the formula of winding perimeter per slot,  $P_{\text{Wind/Slot}}$ , winding resistance per slot,  $R_{\text{Wind/Slot}}$ , and winding resistance per phase,  $R_{\text{Phase}}$ .

$$N = \frac{A_{\text{Slot}}}{A_{\text{Wind}}} \times K \quad (1)$$

$$P_{\text{Wind/Slot}} = 2W_{\text{Stat}} + 2L_{\text{Stack}} \quad (2)$$

$$R_{\text{Wind/Slot}} = P_{\text{Wind/Slot}} \times N \times R_0 \quad (3)$$

$$R_{\text{Phase}} = 6 R_{\text{Wind/Slot}} \quad (4)$$

Were,  $A_{\text{Slot}}$  : single slot area ( $\text{m}^2$ ),  $A_{\text{Wind}}$  : copper wire cross sectional area ( $\text{m}^2$ ),  $K$  : slot fill factor,  $R_0$  : resistivity copper wire ( $\Omega/\text{m}$ ), and  $R_{\text{Wind/Slot}}$  : resistance per slot ( $\Omega$ ). The total winding resistance  $R$  can be derived from two phases winding resistance  $R_{\text{Phase}}$  in series circuit condition as per (5).

$$R = 2 R_{\text{Phase}} \quad (5)$$

Were,  $R_{\text{Phase}}$  : phase resistance ( $\Omega$ ).

## 2.6. Calculation full curve performance

The proposed structure design in Figure 5 is simulated using various sizes of  $W_{\text{stat}}$ ,  $H_{\text{mag}}$  and  $L_{\text{stack}}$ . The analytical simulation begins with CAD and FEA modelling of the stator portion. Under this condition, only the stator winding is energized using three types of stator winding turns,  $N$  and the relevant target stator current  $I_{\text{stat}}$  in order to achieve 600 At and 1400 At of magnetomotive force,  $F_m$ . The outcome value of stator flux density  $B_{\text{stat}}$  is plotted against  $I_{\text{stat}}$  and the decision will be made based on the curve gradient condition. Next, the selected  $W_{\text{stat}}$  size in the stator portion will be combined with the rotor portion, and the  $H_{\text{mag}}$  and  $L_{\text{stack}}$  values will be determined using an ideal DC electromagnetic analysis. The static torque,  $T_{\text{static}}$ , and  $B_{\text{stat}}$  will be plotted against the stator current  $I_{\text{stat}}$  and the judgement will be made based on the lowest  $I_{\text{stat}}$  at maximum  $T_{\text{static}}$  with the condition that  $B_{\text{stat}}$  does not exceed 1.8 T. After that, the correlation curve among  $B_{\text{stat}}$ , transient current  $I_{\text{trans}}$ , and electromagnetic transient torque  $T_{\text{trans}}$  is generated using an ideal sinusoidal BEMF current profile. The final design must meet the requirements of  $I_{\text{trans}}$  less than 6 A and  $B_{\text{stat}}$  of less than 1.8 T. Table 4 shows all the variables used in this research paper.

Table 4. Variable parameter

Parameter	Units	Value
Stator Winding Turns, $N$	[turns]	49, 200 and 228
Stator Teeth Width, $W_{\text{stat}}$	[mm]	15, 19 and 25
Stator Current, $I_{\text{stat}}$	[A]	2.63, 3.00, 5.00, 6.13, 7.00, 12.32, and 28.75
Magnetomotive Force, $F_m$	[At]	600 and 1400
Magnet Height, $H_{\text{mag}}$	[mm]	8, 10, 12 and 14
Stack Length, $L_{\text{stack}}$	[mm]	15, 30 and 45
Transient Current, $I_{\text{trans}}$	[A]	1, 3, 5 and 7

Upon the completion of analytical analysis, an appropriate graph torque versus current could be established and the gradient could be represented by the torque constant,  $K_T$  in (6).

$$T = K_T I \quad (6)$$

The motor performance curves for speed,  $\omega$ , current,  $I$ , mechanical output power,  $P$  could be described in (7)-(9).

$$\omega = \frac{V}{K_e} - \frac{R}{K_T K_e} T \quad (7)$$

$$I = \frac{1}{K_T} T \quad (8)$$

$$P = \frac{VT}{K_e} - \frac{R}{K_T K_e} T^2 \quad (9)$$

Were,  $K_T$  : torque constant (Nm/A),  $I$  : current (A),  $V$  : voltage (V),  $K_e$  : back EMF constant (V/m/s),  $R$  : resistance ( $\Omega$ ), and  $T$  : output torque (Nm).

### 3. RESULT AND DISCUSSION

#### 3.1. Analytical analysis

In this section, the motor has been set to various current loading conditions. Section 3.1.1 focus on the  $W_{\text{stat}}$  variable at the stator portion, and section 3.1.2 focus on  $H_{\text{mag}}$  and  $L_{\text{stack}}$  variables at the rotor portion. Then, the optimum motor design can be determined and the torque constant  $K_T$  can be derived from FEA analytical graph for full curve motor performance.

##### 3.1.1. Electromagnetic analysis stator

Two  $F_m$  conditions are used in this section, 600 At and 1400 At as per Figure 8. The analysis was performed under no loading conditions and with no interaction between stator and rotor. The 15 mm  $W_{\text{stat}}$  is easily saturated when the current reaches 6 A, but for the 25 mm  $W_{\text{stat}}$ , it is hard to be saturated even when the current reaches 28 A. For 19 mm  $W_{\text{stat}}$ , the stator teeth start to be saturated at 7 A and show an acceptable flux density condition for current less than 7 A.

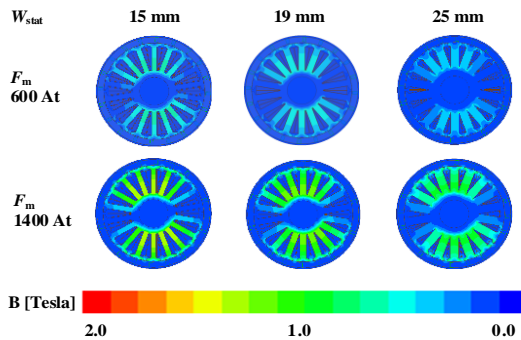


Figure 8. Stator flux density

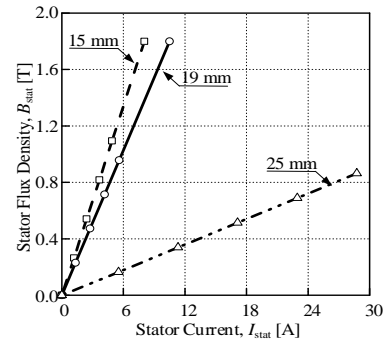


Figure 9. Stator flux density characteristic

By plotting  $B_{\text{stat}}$  versus  $I_{\text{stat}}$  as per Figure 9, the electromagnetic characteristic curve gets less stiff when a large value of  $W_{\text{stat}}$  is used, but more current injection is required to generate sufficient stator flux density. This is due to a lack of winding turns around the teeth and a lack of space. A similar situation occurred with a small value of  $W_{\text{stat}}$ , where stator teeth could be easily saturated even with a small value of current. As a result, a 19 mm  $W_{\text{stat}}$  is the ideal size to be used due to sufficient electromagnetic energy with a current of less than 6 A. The data shows an early confidence level toward 19 mm  $W_{\text{stat}}$  and is good to be used in the next section analysis.

##### 3.1.2. Electromagnetic analysis rotor

The selected 19 mm  $W_{\text{stat}}$  is used with variable parameters from  $H_{\text{mag}}$ ,  $L_{\text{stack}}$  and  $I_{\text{stat}}$ . Figure 10 shows the analytical performances of  $T_{\text{static}}$ ,  $B_{\text{stat}}$  and  $I_{\text{stat}}$ . The plotted graphs are separated based on the dedicated values of 8 mm  $H_{\text{mag}}$ , at Figure 10(a), 10 mm  $H_{\text{mag}}$ , at Figure 10(b), 12 mm  $H_{\text{mag}}$  at Figure 10(c), and 14 mm  $H_{\text{mag}}$ , at Figure 10(d). All the performance analyses are using DC injection.

In every graph, there is a common trend in  $T_{\text{static}}$  and  $B_{\text{stat}}$ . The  $T_{\text{static}}$  increases when the  $L_{\text{stack}}$  and  $I_{\text{stat}}$  are increased. However, the increment in the  $B_{\text{stat}}$  value is contributed by  $I_{\text{stat}}$  alone. This indicates that the flux density saturation at  $B_{\text{stat}}$  is independent of the stack length. When performing a comparison among all four graphs, the electromagnetic energy increases when the  $H_{\text{mag}}$  is increased. The 14 mm  $H_{\text{mag}}$  in Figure 10(d) can produce up to 125 Nm of torque at 7 A current when using a 50 mm  $L_{\text{stack}}$ . The vice versa situation occurs on  $B_{\text{stat}}$  in Figures 10(a)-(c), where the curve is shifted downward when  $H_{\text{mag}}$  is increased, and this gives further margin toward higher  $I_{\text{stat}}$  loading conditions. After going through all the available configurations, the preferable solution is to use 14 mm  $H_{\text{mag}}$  with a 30 mm  $L_{\text{stack}}$ . The design could achieve target output torque ( $T_{\text{static}} > 35$  Nm) at the lowest current ( $I_{\text{stat}} = 3$  A DC), and the flux density is below the saturation level at 1.8 T ( $B_{\text{stat}} = 1.2136$  T) as shown in Table 5. This configuration has been selected for further analysis in the transient condition.

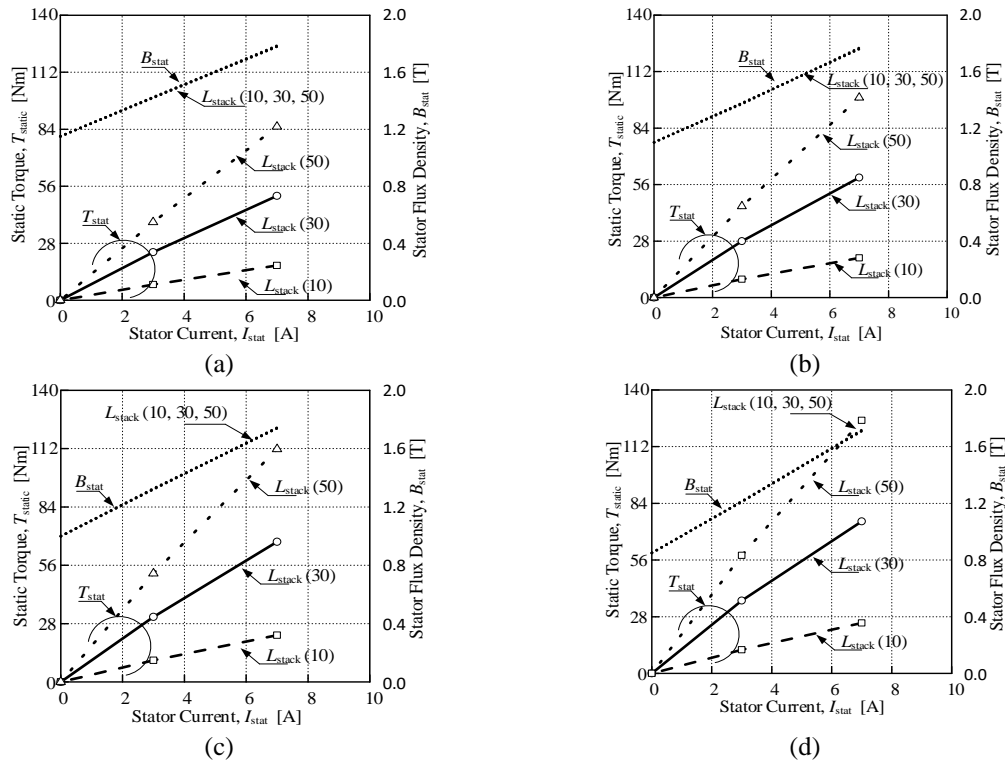


Figure 10. Static characteristic of 19 mm Wstat: (a) 8 mm  $H_{mag}$ , (b) 10 mm  $H_{mag}$ , (c) 12 mm  $H_{mag}$ , and (d) 14 mm  $H_{mag}$

Table 5. Model selection

$H_{mag}$ [mm]	$I_{static}$ [A]	$L_{stack}$ [mm]	$T_{static}$ [Nm]	$B_{stat}$ [T]
8	3	50	38.3	1.4250
10	4	30	36.0	1.4700
12	4	30	40.0	1.4300
14	3	30	36.0	1.2136

The preferable configuration is further analysis using the BEMF current profile that simulates the design in transient conditions. Figure 11 shows the analytical performance among  $T_{trans}$ ,  $B_{stat}$ , and  $I_{trans}$ . The model delivers the 35 Nm torque at 2.62 A ( $I_{trans}$ ) current and 1.59 T ( $B_{stat}$ ) flux density as shown in Table 6. The transient  $I_{trans}$  value is lower than the static  $I_{stat}$  value because all three phases are energised according to waveform commutation, whereby in static analysis, only two phases are energised and the remaining one phase remains ideally zero. This finding allows for an early judgement to be made on the worst condition without spending too much resources on transient simulation. As a result, the selected model of 14 mm  $H_{mag}$  and 30 mm  $L_{stack}$  is accepted for further assessment in full curve performance analysis.

### 3.2. Full curve motor performance

In order to determine the full curve function in terms of torque value, the torque constant  $K_T$  in (1) has to be calculated first from the gradient curve of torque versus current in Figure 11. In this case, the torque constant  $K_T$  value is determined from the FEA transient analysis result based on a series of transient current loadings and using the custom design model, which is close to the actual motor condition. There are another two constants that are required prior to the determination of full curve performance, BEMF constant  $K_e$  and total resistance  $R$ . The BEMF constant  $K_e$  can be calculated directly from the torque constant  $K_T$  value, and the total resistance  $R$  can be estimated from the winding space area in Figure 7 and then calculated using (5) to (9). Upon having all these three constants, the full curve motor performance of speed, current, and output power can be generated as per Figure 12. Based on the curve generation, the motor design is capable of delivering a maximum output power of 703 W with a free running speed of 113 RPM and a stall current of 22.6 A. In terms of rated condition, the design is capable of meeting the target requirement with a rated speed of 96 RPM, a rated current of 3.2 A and a rated output power of 357 W. Table 7 shows the summary finding, and the outcome result shows promising data for the application used.



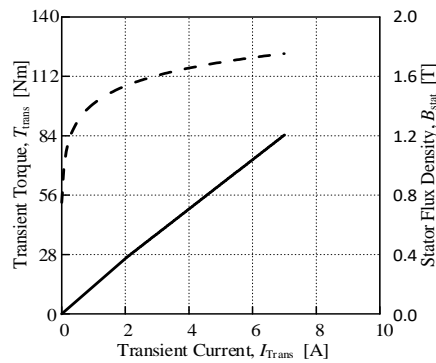


Figure 11. Characteristic of selected model

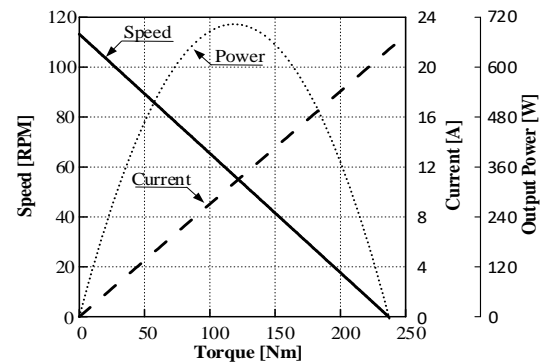


Figure 12. Full curve motor performance

Table 6. Transient analysis result

Parameter	$T_{\text{Trans}}$ [Nm]	$I_{\text{Trans}}$ [A]	$B_{\text{sat}}$ [T]
Value	35	2.62	1.59

Table 7. Summary motor performance

Parameter	Unit	Requirement	Design
Speed, $n$	[rpm]	< 100	96
Current, $I$	[A]	< 6	3.2
Torque, $T$	[Nm]	35	35
Flux Density, $B$	[T]	< 1.8	1.6

#### 4. CONCLUSION

There are several methods to simulate the overall motor performance, but the design limitations of template-based software can lead to inaccurate judgement and early design errors. Too much reliance on FEA analysis will cause a long lead time in motor design development. Hence, an appropriate balance approach between FEA and mathematical equations has to be considered. Therefore, this paper presents a generic method for using FEA for analytical analysis prior to the generation of full curve motor performance using a mathematical equation. The critical torque constant  $K_T$  value in equation 1 is determined from the FEA result, and the total resistance  $R$  value is estimated from the winding space area in the actual motor design condition. These two constants are determined as precisely as possible prior to the generation function of full curve motor performance for speed, current, and output power in terms of torque value. All the rated conditions, including free running speed, maximum output power, and stall current, are verified as a whole package for design review prior to design fabrication and provide an opportunity for any necessary improvement at an early design stage with minimum cost impact. As a conclusion, this research paper shows a methodology that can be used by any motor designer to produce the optimum motor design prior to the first prototype model creation. The leverage benefit can be gained in robust design as well as low-cost development.

#### ACKNOWLEDGEMENTS

The authors would like to thank Ministry of Higher Education Malaysia, Universiti Teknikal Malaysia Melaka (UTeM) for providing the research grant of MTUN/2019/FKECERIA/MC0003.




#### REFERENCES

- [1] S.-H. Kim, "Brushless direct current motors," in *Electric Motor Control*, Elsevier, 2017, pp. 389–416.
- [2] M. A. Khalid, R. N. F. K. R. Othman, N. A. M. Zuki, F. A. A. Shukor, M. N. Othman, and C. A. Vaithilingam, "Performance analysis of brushless dc motor with optimum magnetic energy for bicycle application," *Int. J. Power Electron. Drive Syst.*, vol. 12, no. 4, pp. 2113–2122, 2021, doi: 10.11591/ijpeds.v12.i4.pp2113-2122.
- [3] L. Li and Q. Liu, "Research on IPMSM drive system control technology for electric vehicle energy consumption," *IEEE Access*, vol. 7, pp. 186201–186210, 2019, doi: 10.1109/ACCESS.2019.2958944.
- [4] M. A. Ibrahim, A. K. Mahmood, and N. S. Sultan, "Optimal PID controller of a brushless DC motor using genetic algorithm," *Int. J. Power Electron. Drive Syst.*, vol. 10, no. 2, pp. 822–830, 2019, doi: 10.11591/ijpeds.v10.i2.pp822-830.
- [5] M. Dasari, A. S. Reddy, and M. V. Kumar, "GA-ANFIS PID compensated model reference adaptive control for BLDC motor," *Int. J. Power Electron. Drive Syst.*, vol. 10, no. 1, p. 265, Mar. 2019, doi: 10.11591/ijpeds.v10.i1.pp265-276.




- [6] M. Oh and I. Husain, "Optimal Torque Distribution of Dual-Motor All-Wheel Drive Electric Vehicles for Maximizing Motor Energy Efficiency," in *2021 IEEE Transportation Electrification Conference & Expo (ITEC)*, Jun. 2021, pp. 188–193, doi: 10.1109/ITEC51675.2021.9490089.
- [7] S. Leitner, H. Gruebler, and A. Muetze, "Low-Cost BLDC Claw-Pole Motor Design for Fan Applications with Reduced Cogging Torque and Balanced Axial Forces," *Conf. Proc. - IEEE Appl. Power Electron. Conf. Expo. - APEC*, vol. 2020-March, pp. 279–284, 2020, doi: 10.1109/APEC39645.2020.9124114.
- [8] K. Indirajith and R. B. Kumar, "a Comparative Study of the Transverse , Axial and Radial Flux Pm Synchronous Motors for Wind Application," pp. 944–955.
- [9] N. Baloch, B. Il Kwon, and Y. Gao, "Low-Cost High-Torque-Density Dual-Stator Consequent-Pole Permanent Magnet Vernier Machine," *IEEE Trans. Magn.*, vol. 54, no. 11, 2018, doi: 10.1109/TMAG.2018.2849082.
- [10] S. Garip and Y. Yasa, "Design of Outer Runner-Type Brushless Permanent Magnet DC Motor for Lightweight E-Vehicles," *Proc. - 2020 6th Int. Conf. Electr. Power Energy Convers. Syst. EPECS 2020*, pp. 151–156, 2020, doi: 10.1109/EPECS48981.2020.9304967.
- [11] K. L. Shenoy and M. S. Kumar, "Design topology and electromagnetic field analysis of Permanent Magnet Brushless DC motor for electric scooter application," *Int. Conf. Electr. Electron. Optim. Tech. ICEEOT 2016*, pp. 1541–1545, 2016, doi: 10.1109/ICEEOT.2016.7754942.
- [12] K. Daukaev, A. Rassolkin, A. Kallaste, T. Vaimann, and A. Belahcen, "A review of electrical machine design processes from the standpoint of software selection," *58th Annu. Int. Sci. Conference Power Electr. Eng. Riga Tech. Univ. RTUCON 2017 - Proc.*, vol. 2017-November, pp. 1–6, 2017, doi: 10.1109/RTUCON.2017.8124818.
- [13] T. M. Masuku, R. J. Wang, M. C. Botha, and S. Gerber, "Design Strategy of Traction Induction Motors," *Proc. - 2019 South African Univ. Power Eng. Conf. Mechatronics/Pattern Recognit. Assoc. South Africa, SAUPEC/RobMech/PRASA 2019*, pp. 316–321, 2019, doi: 10.1109/RoboMech.2019.8704761.
- [14] Y. L. Karnavas, I. D. Chasiotis, and D. N. Stravoullellis, "A practical BLDC motor design procedure for diver propulsion vehicle applications," *Proc. - 2018 23rd Int. Conf. Electr. Mach. ICEM 2018*, pp. 513–519, 2018, doi: 10.1109/ICELMACH.2018.8507046.
- [15] N. Murali, S. Ushakumari, V. P. Mini, and A. T. Varghese, "Sizing and performance analysis of an electric motor in an e-rickshaw," *2020 IEEE Int. Conf. Power Syst. Technol. POWERCON 2020*, 2020, doi: 10.1109/POWERCON48463.2020.9230564.
- [16] Y. Verma and M. S. Manna, "Simulation based analysis of outer rotor brushless DC motor for electric vehicle application," *Proc. 2021 8th Int. Conf. Comput. Sustain. Glob. Dev. INDIACom 2021*, pp. 746–751, 2021, doi: 10.1109/INDIACom51348.2021.00133.
- [17] K. Hu and G. Zhang, "Design and Vibration Optimization of Direct Current Motor of Permanent Magnet of Rectangular Magnetic Steel," *IEEE Access*, vol. 8, pp. 126606–126614, 2020, doi: 10.1109/ACCESS.2020.3008214.
- [18] S. K. Chawrasia, C. K. Chanda, and S. Banerjee, "Design and Analysis of In-Wheel Motor for an Electric Vehicle," *2020 IEEE Calcutta Conf. CALCON 2020 - Proc.*, pp. 351–355, 2020, doi: 10.1109/CALCON49167.2020.9106538.
- [19] A. J. Ali, A. H. Ahmed, and B. M. Saied, "Cogging torque Mitigation for PMSM using stator slots design and Magnets skewing," *2nd Int. Conf. Electr. Commun. Comput. Power Control Eng. ICECCPCE 2019*, pp. 240–245, 2019, doi: 10.1109/ICECCPCE46549.2019.203781.
- [20] H. Jigang, F. Hui, and W. Jie, "A PI controller optimized with modified differential evolution algorithm for speed control of BLDC motor," *Automatika*, vol. 60, no. 2, pp. 135–148, 2019, doi: 10.1080/00051144.2019.1596014.
- [21] C. Mohankrishna et al., "Modelling and Simulation of BLDC Motor Using State Space Approach," *Int. J. Innov. Res. Electr. Electron. Instrum. Control Eng.*, vol. 4, no. 5, pp. 2321–2526, 2016.
- [22] A. Rawat, M. Bilal, and M. F. Azeem, "PI Controller Based Performance Analysis of Brushless DC Motor, Utilizing MATLAB Simulink Environment," *J. Sci. Res. Reports*, pp. 38–43, 2020, doi: 10.9734/jsrr/2020/v26i230222.
- [23] M. J. Bala, D. Roy, and A. Sengupta, "The Performance Enhancement of BLDC Motor Using Halbach Array Rotor," *2020 IEEE Int. Conf. Conver. Eng. ICCE 2020 - Proc.*, pp. 405–409, 2020, doi: 10.1109/ICCE50343.2020.9290642.
- [24] B. Azhari, P. Irasari, and P. Widiyanto, "Design and simulation of 5kw bldc motor with half-buried permanent magnets using an existing stator body," *Int. J. Power Electron. Drive Syst.*, vol. 12, no. 4, pp. 2030–2043, 2021, doi: 10.11591/ijpeds.v12.i4.pp2030-2043.
- [25] P. K. Shahri, V. Izadi, and A. H. Ghasemi, "Design a High Efficiency and Low Ripple BLDC Motor Based on Multi-Objective Optimization Methods," *Proc. Am. Control Conf.*, vol. 2020-July, pp. 156–161, 2020, doi: 10.23919/ACC45564.2020.9147907.
- [26] A. M. Ajamloo, A. Ghaheri, and E. Afjei, "Multi-objective Optimization of an Outer Rotor BLDC Motor Based on Taguchi Method for Propulsion Applications," *2019 10th Int. Power Electron. Drive Syst. Technol. Conf. PEDSTC 2019*, pp. 34–39, 2019, doi: 10.1109/PEDSTC.2019.8697586.
- [27] D. Staton, "Thermal analysis of traction motors," in *2014 IEEE Transportation Electrification Conference and Expo (ITEC)*, Jun. 2014, pp. 1–139, doi: 10.1109/ITEC.2014.6861820.
- [28] N. Abdullah, R. N. F. R. Othman, K. A. Karim, and L. S. Tat, "Analysis on EMF characteristics for torque ripple reduction in BLAC motor intended for HVLS fan application," *Int. J. Power Electron. Drive Syst.*, vol. 11, no. 4, pp. 2203–2211, 2020, doi: 10.11591/ijpeds.v11.i4.pp2203-2211.

## BIOGRAPHIES OF AUTHORS






**Saharudin Kamaroszaman**    was born on 18 September 1986 at Johor Bahru, Johor, Malaysia. In 2011, he received his Bachelor's degree in Mechanical Engineering from University of applied Science Albstadt Sigmaringen, Germany. Currently, he is pursuing her study in Master of Science in Electrical Engineering at Universiti Teknikal Malaysia Melaka (UTeM). His research study is in machine design. He can be contacted at email: m011920010@student.utem.edu.my.






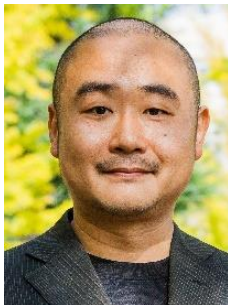
**Raja Nor Firdaus Kashfi Raja Othman**    was born in Parit Buntar, Perak, Malaysia on May 2, 1982. In 2006, 2009, and 2013, he got his B.Eng., M.Sc., and Ph.D. in Electrical Power Engineering from Universiti Putra Malaysia, respectively. He is currently an Associate Professor at Universiti Teknologi Malaysia Melaka's Department of Electrical Engineering, Faculty of Electrical Engineering. Applied magnetics, electrical machines, magnetic sensors, and drives are among his scientific interests. He can be contacted at email: norfirdaus@utem.edu.my.






**Kasrul Abdul Karim**    earned an M.Sc. from the University of Bradford in 2003 and a PhD from the University of Nottingham in the United Kingdom in 2011. He is currently an Associate Professor at Universiti Teknologi Malaysia Melaka's Faculty of Electrical Engineering. Electrical machine design, power electronics, and electrical vehicle design are among his research interests. He can be contacted at email: kasrul@utem.edu.my.



**Suhairi Rizuan Che Ahmad**    was born in Kota Bharu, Kelantan, on June 13, 1984. In 2009, he got a B. Eng. in Industrial Electronics from Universiti Malaysia Perlis, Malaysia, and in 2012, he received an M. Sc. in Electrical Power Engineering from Universiti Putra Malaysia. In 2019, he obtained his PhD in electrical machine design from Universiti Teknikal Malaysia Melaka. His research interests include electrical machine design, modeling of electric machines, electric drives, energy conversion, and renewable energy. He can be contacted at email: suhairir@unikl.edu.my.



**Kunihisa Tashiro**    earned his B.Eng. and M.Eng. degrees from Kanazawa University in Japan in 1998 and 2000, respectively. He worked as a Research Assistant at Kyushu University in Japan from 2000 to 2006, where he earned his Ph.D. (Eng.) in 2006. He began as an Assistant Professor in the Department of Electrical and Computer Engineering, Faculty of Engineering, Shinshu University, Japan, in 2006, and was promoted to Associate Professor in 2012. From 2012 to 2019, he was the director of Shinshu University's Magnetic Energy Harvesting Project. His research interests include INNO-vation research with electromagnetic phenomena, such as the use of magnetic energy as a sensor, actuator, and shield. He is a Senior Member of the Japanese Institute of Electrical Engineering (IEEE) and a Director of the Japan Society of Applied Electromagnetics and Mechanics (AEM). He is currently the head, investigating R&D Committee on magnetic sensor with machine learning (AMAG1209) in IEEE. He also serves on various technical committees, AMAG1203 (Biomagnetics) and AEMC1049 (IoT and EMC) of IEEE, and other academic society. He can be contacted at email: tashiro@shinshu-u.ac.jp.